Disordered Exciton Model for the Core Light-Harvesting Antenna of *Rhodopseudomonas viridis*

Vladimir Novoderezhkin,* René Monshouwer,# and Rienk van Grondelle#

*A. N. Belozersky Institute of Physico-Chemical Biology, Moscow State University, Moscow 119899, Russia, and #Department of Biophysics, Faculty of Sciences, Vrije Universiteit, 1081 HV Amsterdam, the Netherlands

ABSTRACT In this work we explain the spectral heterogeneity of the absorption band (Monshouwer et al., 1995. *Biochim. Biophys. Acta.* 1229:373–380), as well as the spectral evolution of pump-probe spectra for membranes of *Rhodopseudomonas* (*Rps.*) *viridis*. We propose an exciton model for the LH1 antenna of *Rps. viridis* and assume that LH1 consists of 24–32 strongly coupled BChl *b* molecules that form a ring-like structure with a 12- or 16-fold symmetry. The orientations and pigment-pigment distances of the BChls were taken to be the same as for the LH2 complexes of BChl *a*–containing bacteria. The model gave an excellent fit to the experimental results. The amount of energetic disorder necessary to explain the results could be precisely estimated and gave a value of 440–545 cm^{-1} (full width at half-maximum) at low temperature and 550–620 cm^{-1} at room temperature. Within the context of the model we calculated the coherence length of the steady-state exciton wavepacket to correspond to a delocalization over 5–10 BChl molecules at low temperature and over 4–6 molecules at room temperature. Possible origins of the fast electronic dephasing and the observed long-lived vibrational coherence are discussed.

INTRODUCTION

The primary processes of photosynthesis include the absorption of solar photons by the pigments of the light-harvesting antenna, followed by ultrafast energy transfer until a reaction center is reached in which a charge separation can be initiated (van Grondelle, 1985; van Grondelle et al., 1994; Sundström et al., 1999). Recent advances in high-resolution structural studies of bacterial light-harvesting antenna systems (McDermott et al., 1995; Koepke et al., 1996; Hu et al., 1997) have strongly stimulated experimental and theoretical investigations to unravel the fundamental physical principles that are the basis for the very efficient energy transfer in these antenna complexes. From the structural and earlier biochemical (Zuber and Cogdell, 1995) studies it is now well established that antenna complexes of purple bacteria consist of α-β pigment-protein subunits arranged in high-symmetry ring-like structures. Each subunit consists of a pair of transmembrane polypeptides, α and β, binding two or three bacteriochlorophyll (BChl) molecules, and in some species a third polypeptide γ was identified (Zuber and Brunisholz, 1991). The spatial organization of the pigments in these rings is currently known with high precision in two peripheral LH2 complexes (McDermott et al., 1995; Koepke et al., 1996); all extensions to other complexes (in particular the core complex LH1) are educated guesses (Hu et al., 1997). Although the spatial organization is known, the nature of the spectra and dynamics of electronic excitations still remains unclear.

Using the structural parameters from the x-ray data, several groups have modeled the exciton spectra of these ring-like complexes, taking into account the site inhomogeneity of the pigments (Dracheva et al., 1996, 1997; Jimenez et al., 1996; Sauer et al., 1996; Alden et al., 1997; Monshouwer et al., 1997; Hu et al., 1997; Wu et al., 1997a,b). Different estimations of the interaction energy and the site inhomogeneity values in these papers have resulted in different predictions for the degree of exciton delocalization in the light-harvesting antenna. A direct estimate of the delocalization degree is obtained from the shape and amplitude of difference absorption spectra (Novoderezhkin and Razjivin, 1993; Van Burgel et al., 1995; Pullerits et al., 1996). Analysis of the room-temperature pump-probe spectra for the LH2 antenna complexes of purple bacteria suggests exciton delocalization over four BChls (Pullerits et al., 1996; Kühn and Sundström, 1997). Relative difference absorption measurements of the LH2 antenna and the B820 dimeric subunit revealed delocalization over five BChls (Novoderezhkin et al., manuscript submitted for publication). Analysis of the shapes and relative amplitudes of difference absorption of the B866 band and the B808 monomeric band of the B808–866 complex from green bacteria (analogous to LH2) gave a delocalization value of about five or six BChls (Novoderezhkin and Fetisova, manuscript submitted for publication). From nonlinear absorption experiments an even larger delocalization degree was proposed (Leupold et al., 1996).

Probably the most special and mysterious among all of the species of purple bacteria is the BChl *b*–containing bacterium *Rhodopseudomonas* (*Rps.*) *viridis.* Electron microscopy studies have shown a regular circular organization of the LH1 antenna (Miller, 1982; Stark et al., 1984; Ikedayamasaki et al., 1998) around the reaction center. The

Received for publication 14 December 1998 and in final form 28 April 1999.

Address reprint requests to Dr. Rienk van Grondelle, Faculty of Physics and Astronomy, Vrije Universiteit, De Boelelaan 1081, 1081 HV Amsterdam, the Netherlands. Tel.: 31-20-444-7930; Fax: 31-20-444-7999; E-mail: rienk@nat.vu.nl.

0006-3495/99/08/666/16 $2.00

main absorption band around 1000 nm is very redshifted and was found to be heterogeneous, with at least three spectral bands contributing to the major LH1 peak (Monshouwer et al., 1995). The corresponding maxima of the second derivative of the membrane absorption spectrum at 4.2K are 1049, 1042, and 1030 nm. This is in remarkable contrast to the LH1 absorption band of BChl *a*–containing species (van Mourik et al., 1992).

Low-temperature emission spectra of membranes of *Rps. viridis* were studied for different excitation wavelengths (Monshouwer et al., 1995). The shape of the red edge of the emission spectrum and the position of the maximum of the emission (1054 nm) do not change when the excitation wavelength is tuned from the blue to the red edge of the absorption band (from 1018 to 1047 nm). Polarization of the emission for these excitation wavelengths is constant ($r = 0.1$) and only starts to increase upon excitation in the very red edge (from 1050 nm). All of these data strongly suggest very efficient excitation transfer (or relaxation) to the redmost pigment pool (or exciton level), which was denoted as the B1045 spectral form (Monshouwer et al., 1995).

Recently, time-resolved pump-probe measurements of membranes of *Rps. viridis* were performed at different temperatures (Monshouwer et al., 1998). It was found that the major relaxation processes take place within the first picosecond after excitation. The ultrafast redshift of the difference absorption spectrum (with a time constant of ~130 fs) accompanied by an anisotropy decay (time constant of 150 fs) were taken to reflect the electronic energy transfer and dephasing processes. The coupling of the electronic transitions with two vibrational modes (65 and 103 cm^{-1}) gives rise to strong oscillations at all detection wavelengths and all temperatures. The surprisingly long decay of these oscillations (700–800 fs) indicates that the ultrafast electronic energy transfer does not shorten the vibronic dephasing.

In this paper we have modeled the linear absorption and pump-probe spectra obtained by Monshouwer et al. (1998), using an exciton model for the LH1 antenna of *Rps. viridis*. The spectral heterogeneity of the LH1 antenna was explained in terms of the exciton splitting of the major electronic transition due to resonant interactions in a ring-like aggregate of BChls. Within the context of this model, we calculated the degree of exciton delocalization at different temperatures, using the site inhomogeneity value and the other parameters obtained from a simultaneous fit of absorption and pump-probe spectra.

MODEL OF ANTENNA

The elementary subunit of the core antenna of *Rps. viridis* consists of three transmembrane polypeptides α, β, and γ (Miller, 1982; Stark et al., 1984; Zuber and Brunisholz, 1991). The α and β polypeptides, binding one BChl molecule each, are analogous to the LH1 proteins found in BChl *a*–containing bacteria. The γ-polypeptide probably does not bind BChl (Zuber and Brunisholz, 1991). The available structural information suggests that the photosynthetic unit of *Rps. viridis* consists of one reaction center surrounded by six antenna subunits ($\alpha_2\beta_2\gamma_2BChl_4$) (each containing two α, two β, and two γ polypeptides and four BChls) arranged in a ring-like structure with sixfold symmetry. The spatial arrangement of the BChls should have at least the same (sixfold) or even higher (12-fold) symmetry (the exact nature of the BChl organization in this antenna complex is not known). Alternatively, the LH1 may be a 16-fold symmetrical ring of 16 ($\alpha\beta\gamma BChl_2$) subunits, as was shown to be the case for the BChl *a*–containing species (Karrasch et al., 1995; Walz et al., 1998). In this case the spatial arrangement of the BChls should also exhibit 16-fold symmetry.

We suppose that the pigment arrangement in the antenna of *Rps. viridis* is analogous to that of the BChl *a*–containing bacteria. As a model for the antenna of *Rps. viridis* we consider a circular aggregate of 24–32 BChl *b* molecules with either C_{12} or C_{16} symmetry (the elementary unit cell contains two BChl *b* molecules, bound to the α- and β-polypeptides). The Q_y transition dipole moments of the two BChls in a dimeric unit cell form angles ψ_1, ψ_2 with the plane of the circle and angles φ_1, φ_2 with the tangent to the circle (ψ_1 and ψ_2 take values from $-90°$ to $90°$; φ_1 and φ_2 from $0°$ to $360°$). The unperturbed Q_y electronic transition energies of these two BChls are E_1 and E_2. The Mg-Mg distance between BChls in a dimeric unit is r_{12} and between nearest BChls from different units is r_{23}. We further assume that $\psi_1 = 10°$, $\psi_2 = 5°$, $\varphi_1 = 20°$, $\varphi_2 = 200°$, $r_{12} = 0.87$ nm, $r_{23} = 0.97$ nm. These parameters are approximately the same as those for the strongly coupled B850 ring of BChl *a*'s in the LH2 antenna from *Rhodopseudomonas* (*Rps.*) *acidophila* (McDermott et al., 1995). The difference between E_1 and E_2 was varied from 0 to 600 cm^{-1}. The ratio of the transition dipoles for the S_1-S_2 and S_0-S_1 transitions in the BChl monomer, χ, was varied from 0 to 1.5. In our simulations of the long-wavelength absorption band, we have taken into account the interactions between the Q_y transitions of BChls, neglecting their mixing with Q_x, B_y, B_x transitions as well as with charge transfer states (Alden et al., 1997).

We have assumed that the interaction energies between BChl *b* molecules are $M_{12} = 400$ cm^{-1}, $M_{23} = 290$ cm^{-1}, and $M_{13} = -52$ cm^{-1}, where M_{12} corresponds to the intradimer interaction, M_{23} to the interdimer nearest-neighboring interaction, and M_{13} to the next nearest-neighbor interaction, respectively. Furthermore, we tested two alternative sets of interaction energies: "high" energies, $M_{12} = 600$ cm^{-1}, $M_{23} = 440$ cm^{-1}, $M_{13} = -78$ cm^{-1}, and "low" energies, $M_{12} = 260$ cm^{-1}, $M_{23} = 190$ cm^{-1}, $M_{13} = -34$ cm^{-1}. Note that microscopic calculations using the point charge approximation gave $M_{12} = 806$ cm^{-1}, $M_{23} = 377$ cm^{-1}, $M_{13} = -152$ cm^{-1} for the LH2 complex of *Rhodospirillum molischianum* (Hu et al., 1997), and $M_{12} = 197$–545 cm^{-1}, $M_{23} = 158$–461 cm^{-1}, with various treatments of the dielectric screening for the LH2 complex of *Rps. acidophila* (Alden et al., 1997). For the LH2 complex of *Rhodobacter* (*Rb.*) *sphaeroides*, an analysis of the exper-

TABLE 1 Energies (E) and dipole strengths (D_x, D_y, D_z, $D = D_x + D_y + D_z$) of one-exciton transitions calculated for the LH1 antenna

E (cm^{-1})	D_x	D_y	D_z	D	E (cm^{-1})	D_x	D_y	D_z	D
(a) $\sigma = 0$, $E_1 - E_2 = 0$					(c) $\sigma = 440$ cm^{-1}, $E_1 - E_2 = 0$				
−806.0000	0.0000	0.0000	0.0449	0.0449	−905.5264	2.0564	2.0340	0.0223	4.1127
−768.4823	11.7640	0.0071	0.0000	11.7712	−834.8576	3.6292	3.6300	0.0100	7.2692
−768.4823	0.0071	11.7640	0.0000	11.7712	−779.4213	3.5833	3.6019	0.0072	7.1924
−661.4439	0.0000	0.0000	0.0000	0.0000	−705.3842	0.9423	0.9667	0.0029	1.9119
−661.4439	0.0000	0.0000	0.0000	0.0000	−649.6405	0.7453	0.7222	0.0021	1.4696
−500.4078	0.0000	0.0000	0.0000	0.0000	−540.8028	0.2273	0.2315	0.0012	0.4600
−500.4078	0.0000	0.0000	0.0000	0.0000	−481.7954	0.1863	0.1839	0.0010	0.3711
−308.4028	0.0000	0.0000	0.0000	0.0000	−348.6161	0.0881	0.0877	0.0009	0.1767
−308.4028	0.0000	0.0000	0.0000	0.0000	−288.8738	0.0722	0.0690	0.0009	0.1421
−115.3612	0.0000	0.0000	0.0000	0.0000	−154.0828	0.0391	0.0398	0.0012	0.0801
−115.3612	0.0000	0.0000	0.0000	0.0000	−93.2541	0.0385	0.0396	0.0013	0.0794
2.0000	0.0000	0.0000	0.0000	0.0000	13.4980	0.0321	0.0326	0.0016	0.0662
210.0000	0.0000	0.0000	0.0000	0.0000	167.4429	0.0159	0.0158	0.0043	0.0360
298.9586	0.0000	0.0000	0.0000	0.0000	252.1265	0.0130	0.0140	0.0053	0.0323
298.9586	0.0000	0.0000	0.0000	0.0000	306.3754	0.0117	0.0124	0.0063	0.0305
414.4028	0.0000	0.0000	0.0000	0.0000	375.3434	0.0099	0.0101	0.0100	0.0299
414.4028	0.0000	0.0000	0.0000	0.0000	423.8295	0.0092	0.0090	0.0134	0.0316
500.4078	0.0000	0.0000	0.0000	0.0000	475.3449	0.0081	0.0086	0.0209	0.0377
500.4078	0.0000	0.0000	0.0000	0.0000	518.8094	0.0090	0.0086	0.0275	0.0451
555.4439	0.0000	0.0000	0.0000	0.0000	560.7907	0.0098	0.0092	0.0393	0.0583
555.4439	0.0000	0.0000	0.0000	0.0000	599.9184	0.0104	0.0098	0.0501	0.0703
584.8850	0.0023	0.0000	0.0000	0.0023	641.9421	0.0103	0.0106	0.0632	0.0841
584.8850	0.0000	0.0023	0.0000	0.0023	688.7488	0.0119	0.0125	0.0761	0.1004
594.0000	0.0000	0.0000	0.4081	0.4081	757.1631	0.0142	0.0139	0.0841	0.1122
(b) $\sigma = 0$, $E_1 - E_2 = 600$ cm^{-1}					(d) $\sigma = 440$ cm^{-1}, $E_1 - E_2 = 600$ cm^{-1}				
−867.5773	0.0000	0.0000	0.0063	0.0063	−979.8353	1.9718	1.9509	0.0022	3.9249
−832.0019	0.0005	11.2931	0.0000	11.2937	−905.2377	3.1377	3.3401	0.0016	6.4794
−832.0019	11.2931	0.0005	0.0000	11.2937	−847.3102	3.2973	3.2084	0.0014	6.5071
−731.3834	0.0000	0.0000	0.0000	0.0000	−776.6938	1.1099	1.0643	0.0009	2.1751
−731.3834	0.0000	0.0000	0.0000	0.0000	−718.3796	0.7900	0.7434	0.0008	1.5342
−583.4449	0.0000	0.0000	0.0000	0.0000	−623.2337	0.2972	0.3128	0.0006	0.6105
−583.4449	0.0000	0.0000	0.0000	0.0000	−562.3780	0.2411	0.2237	0.0005	0.4653
−416.6935	0.0000	0.0000	0.0000	0.0000	−452.8478	0.1138	0.1184	0.0005	0.2327
−416.6935	0.0000	0.0000	0.0000	0.0000	−387.8664	0.0881	0.0917	0.0005	0.1804
−272.7767	0.0000	0.0000	0.0000	0.0000	−289.3488	0.0701	0.0677	0.0007	0.1384
−272.7767	0.0000	0.0000	0.0000	0.0000	−219.5519	0.0681	0.0683	0.0009	0.1373
−211.5154	0.0000	0.0000	0.0000	0.0000	−132.1244	0.0702	0.0658	0.0011	0.1371
423.5154	0.0000	0.0000	0.0000	0.0000	287.3111	0.0066	0.0067	0.0100	0.0234
456.3741	0.0000	0.0000	0.0000	0.0000	366.0013	0.0083	0.0075	0.0100	0.0259
456.3741	0.0000	0.0000	0.0000	0.0000	424.1711	0.0092	0.0100	0.0115	0.0307
522.6935	0.0000	0.0000	0.0000	0.0000	474.0124	0.0149	0.0152	0.0161	0.0462
522.6935	0.0000	0.0000	0.0000	0.0000	518.2216	0.0208	0.0189	0.0205	0.0602
583.4449	0.0000	0.0000	0.0000	0.0000	561.6985	0.0280	0.0269	0.0276	0.0825
583.4449	0.0000	0.0000	0.0000	0.0000	601.7421	0.0356	0.0365	0.0331	0.1052
625.3834	0.0000	0.0000	0.0000	0.0000	640.5047	0.0517	0.0519	0.0444	0.1480
625.3834	0.0000	0.0000	0.0000	0.0000	678.2698	0.0613	0.0679	0.0561	0.1853
648.4045	0.0044	0.4754	0.0000	0.4798	720.0725	0.0794	0.0808	0.0654	0.2256
648.4045	0.4754	0.0044	0.0000	0.4798	769.6431	0.0931	0.0902	0.0723	0.2556
655.5773	0.0000	0.0000	0.4467	0.4467	847.7937	0.1094	0.1055	0.0741	0.2890

$N = 24$, $M_{12} = 400$ cm^{-1}, $M_{23} = 290$ cm^{-1}, $M_{13} = -52$ cm^{-1}; $\sigma = 0$, 440 cm^{-1} and $E_1 - E_2 = 0$, 600 cm^{-1}. The zero of energy is $(E_1 + E_2)/2$. The D_x, D_y, D_z, and D values are normalized to the monomeric dipole strength.

imental CD spectrum yielded $M_{12} = 300$ cm^{-1} and $M_{23} = 233$ cm^{-1} (Koolhaas et al., 1998).

The site inhomogeneity of the LH1 antenna was described by uncorrelated perturbations δE of the electronic energies of the BChl pigments (uncorrelated diagonal disorder). The δE values were randomly taken from a Gaussian distribution $W(\delta E) = \pi^{-1/2}\Delta^{-1}\exp(-\delta E^2/\Delta^2)$. The width (full width at half-maximum, FWHM) of this distribution, $\sigma = 2\Delta(\ln 2)^{1/2}$, was varied from 0 to 1000 cm^{-1}. The Monte Carlo calculations of the linear and nonlinear (pump-probe) absorption spectra included:

1. Direct numerical diagonalization of one- and two-exciton Hamiltonians for 1000–4000 realizations of diagonal energies. We used the standard Hamiltonian for a Fren-

kel exciton in the Heitler-London approximation for three-level molecules. The exciton-phonon interactions were not taken into account.

2. Calculation of the homogeneously broadened spectra from stick spectra (for each set of diagonal energies). We assumed Gaussian line shapes with homogeneous line widths (FWHM) γ_{1L}, γ_{1H}, γ_2, where γ_{1L}, γ_{1H}, γ_2 correspond to transitions to the lowest one-exciton level, to the higher one-exciton levels, and from the one- to the two-exciton levels, respectively. The parameters γ_{1L}, γ_{1H}, γ_2 and the Stokes shift for one-exciton levels are variable, and their optimal values should be determined from the fitting of the experimental data.

3. Averaging of the homogeneously broadened spectra over a random distribution of diagonal energies (convolution of homogeneous and inhomogeneous line shapes).

RESULTS

Exciton structure of a ring with a dimeric unit cell

We start with a study of the structure of one-exciton states of the antenna that are responsible for the linear absorption line shape. In Table 1 the parameters of the one-exciton states for the 12-fold symmetrical circular aggregate are shown for the "normal" set of interaction energies (M_{12} = 400 cm^{-1}, M_{23} = 290 cm^{-1}, and M_{13} = −52 cm^{-1}), in the homogeneous limit ($\sigma = 0$) and in the presence of disorder (σ = 440 cm^{-1}). For both cases we have calculated the exciton structure with either equal or nonequal transition energies of BChls in an α-β unit, i.e., taking $E_1 - E_2 = 0$, and $E_1 - E_2$ = 600 cm^{-1}. The zero of energy is taken to be $(E_1 + E_2)/2$. The dipole strengths D_x, D_y, D_z, $D = D_x + D_y + D_z$ of the exciton components are normalized to the dipole strength of the monomeric S_0-S_1 transition (x and y axes are in the plane of the ring, the z axis is perpendicular to the plane). The dipole strengths are averaged over disorder, for example, D_x for any particular exciton state actually means $\langle D_x \rangle$, where brackets indicate averaging over realizations of diagonal energies. Energies of one-exciton transitions E were calculated as $\langle ED \rangle / \langle D \rangle$, i.e., they correspond to the center of the spectral line (which can be slightly different from the line maximum because of asymmetry of the inhomogeneous line shape).

For a homogeneous aggregate with a dimeric unit cell, the lowest exciton level is the out-of-plane (z-) polarized $k = 0$ level of the lower Davydov component, where k is the exciton wavenumber. The next two are the in-plane polarized twofold degenerate levels, $k = \pm 1$. The higher levels (in increasing order of energy) are the $k = \pm 2, \ldots k = \pm 5$, $k = 6$ levels of the lower Davydov component, and $k = 6$, $k = \pm 5, \ldots \pm 1$, $k = 0$ levels of the higher Davydov component. In the homogeneous model only the $k = 0$ and $k = \pm 1$ levels are dipole allowed. If the angles ψ_1, ψ_2 are small, and the $\varphi_1 - \varphi_2$ value is close to 0° or 180°, then the largest part of the dipole strength of the circular aggregate will be concentrated in the $k = \pm 1$ levels of the lower Davydov component. In this case the $k = 0$ levels of both Davydov components are very weak, and their intensities are proportional to $(\psi_1 - \psi_2)^2$ for the lower and $(\psi_1 + \psi_2)^2$ for the higher Davydov component (see Table 1a). If we increase the asymmetry of the dimeric unit cell by increasing the energy difference, $E_1 - E_2$, this will give rise to a larger Davydov splitting and to some redistribution of dipole strength between the Davydov components (without any changes of the exciton structure within the Davydov components; see Table 1b). The exciton structure within the Davydov components can be changed only by a perturbation that breaks the symmetry of the ring, but not the symmetry within a dimeric unit cell. Such a situation is in fact realized in a spectrally disordered ring. In this case the $k = 0$, $k = \pm 2, \ldots k = \pm 5$, $k = 6$ levels become dipole allowed, borrowing some fraction of the dipole strength from the $k = \pm 1$ levels (see Table 1c). The situation is best described as a mixing of the wavefunctions of the homogeneous aggregate, induced by the site inhomogeneity. Note that the mixture of the $k = \pm 1$ and $k = 0$ wavefunctions results in a change of polarization of the lowest exciton level from out-of-plane to in-plane, together with an increase of its intensity. Another important result concerns the splitting between the $k = \pm 1$ levels as well as the increase in the splitting between these and the lowest $k = 0$ level. For example, in the homogeneous limit the gap between the $k = \pm 1$ and $k = 0$ levels is 38 cm^{-1}, whereas for σ = 440 cm^{-1} the $k = -1$ and $k = 1$ levels are shifted by 71 cm^{-1} and 126 cm^{-1} from the $k = 0$ level (Table 1c). All of these effects of inhomogeneity become more pronounced in the presence of intradimer asymmetry, $E_1 - E_2$ (Table 1d).

The shape of the difference absorption spectra

The shape of the difference absorption spectra as measured in pump-probe spectroscopy is determined by photobleaching (PB) and stimulated emission (SE) of the one-exciton levels and by excited state absorption (ESA) due to transitions from the one- to the two-exciton states. In Fig. 1 the calculated steady-state difference absorption spectrum and its PB, SE, and ESA components are shown (by "steady state" we mean with respect to excitonic and vibrational relaxation in the exited state of the aggregate). In general, the PB and SE spectra consist of N exciton components, whereas the ESA spectrum is a sum of about $N^3/2$ transitions from N one-exciton levels to $N(N + 1)/2$ two-exciton levels. The most intense ESA lines, corresponding to transitions from a few low one-exciton levels, are blue-shifted with respect to the PB/SE lines, giving rise to a specific sigmoid spectrum, which is characteristic for a circular aggregate (Novoderezhkin and Razjivin, 1993, 1995a), as well as for a quasilinear aggregate (Van Burgel et al., 1995; Pullerits et al., 1996).

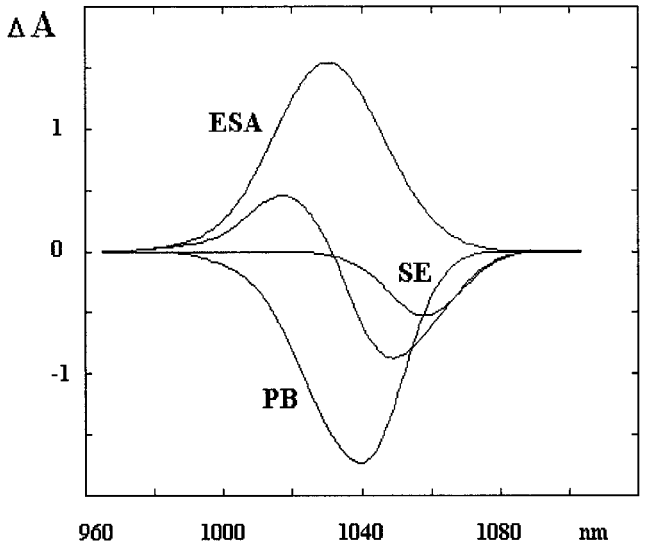

FIGURE 1 The calculated spectral shapes of the photobleaching (PB), stimulated emission (SE), excited state absorption (ESA), and the resulting difference absorption spectrum at 77 K. Parameters correspond to fit no. 3 (see Table 2), i.e., $N = 24$, $M_{12} = 400\ cm^{-1}$, $\gamma_{1L} = 40\ cm^{-1}$, $\gamma_{1H} = 182\ cm^{-1}$, $\gamma_2 = 230\ cm^{-1}$, $\sigma = 440\ cm^{-1}$, $E_1 - E_2 = 0$, and the Stokes shift is $110\ cm^{-1}$.

Simultaneous fit of linear and nonlinear absorption profiles

In Figs. 2–5 the experimental absorption and pump-probe spectra are shown together with the calculated spectra. For this fit we used the steady-state pump-probe spectra measured at 1.6 ps after excitation. Parameters γ_{1L}, γ_{1H}, γ_2, σ, and the value of Stokes shift, which gave the best fit for different N, M_{12}, M_{23}, M_{13}, and $E_1 - E_2$ values are listed in Table 2. Typically, excitonic interactions explain only part of the red shift of the absorption maximum of LH1 with respect to the absorption peak of the BChl *b* monomer. To obtain the correct position of the experimental absorption maximum, we have assumed that the in situ electronic transition energies of both BChl *b*'s in the dimeric unit are $E_1 + \Delta E$ and $E_2 + \Delta E$, where ΔE is a free parameter, different for the fit nos. 1–9 shown in Table 2, but the same for each pair of absorption and pump-probe spectra. The ratio of the transition dipoles for the S_1-S_2 and S_0-S_1 transitions in the BChl monomer, χ, was taken to be 0.5 (for larger χ it is more difficult to reproduce the shape of the pump-probe spectra).

It is remarkable that the fitting parameters in Table 2 vary only slightly when we change the interaction energies or the value of $E_1 - E_2$. For example, for the low-temperature (77 K) absorption and pump-probe spectra, we obtain $\gamma_{1L} = 40\ cm^{-1}$, $\gamma_{1H} = 166–199\ cm^{-1}$, $\gamma_2 = 230\ cm^{-1}$, $\sigma = 370–495\ cm^{-1}$, and the Stokes shift of 100–110 cm^{-1}, upon variation of the interaction energy from 260 to 600 cm^{-1} with $N = 24$. For $N = 32$ all fitting parameters are approximately the same as for $N = 24$, but the disorder value is larger (increasing from 440 to 545 cm^{-1} for the interaction energy of 400 cm^{-1}). For these parameters the shape of the absorption spectrum is dominated by the five lowest exciton components ($k = 0$, $k = \pm 1$, $k = \pm 2$), which have maxima at 1046–1049, 1039–1042, 1032–1036, 1020–1031, and 1012–1025 nm. The lowest component ($k = 0$) has the width of 15–18 nm, and its dipole strength is 3.4–4.1 ($N = 24$) or 4.7–5.5 ($N = 32$), i.e., 14–17% of the total dipole strength of the aggregate in this range of N values. The two higher levels ($k = \pm 1$) are more intense and broader. The next two ($k = \pm 2$) are also broad but much less intense. The additional broadening of the higher levels is explained by additional homogeneous broadening due to relaxation (see the difference between γ_{1L} and γ_{1H}). Notice that within the

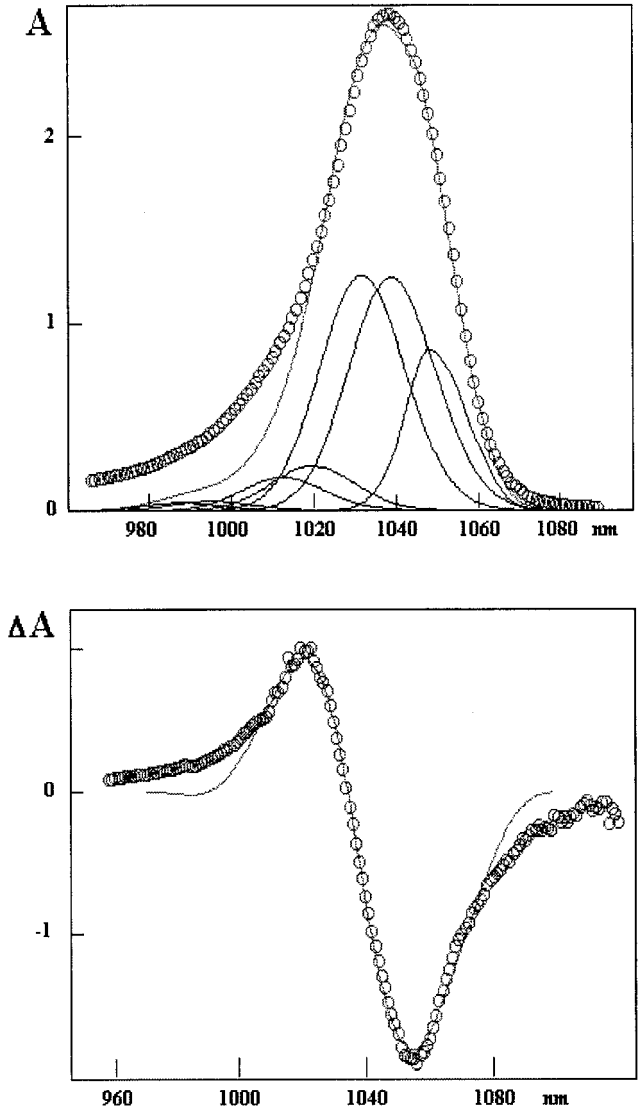

FIGURE 2 Simultaneous fit of linear absorption (*top*) and pump-probe spectra (*bottom*). Circles show experimental data; solid lines show calculated spectra. The absorption profiles for individual exciton components are also shown by solid lines. $T = 77$ K, $N = 24$, $M_{12} = 600\ cm^{-1}$, $\gamma_{1L} = 40\ cm^{-1}$, $\gamma_{1H\ =\ 191\ cm}{}^{-1}$, $\gamma_2 = 230\ cm^{-1}$, $\sigma = 495\ cm^{-1}$, $E_1 - E_2 = 0$, and the Stokes shift is $105\ cm^{-1}$ (fit no. 1). The ΔA values are in arbitrary units.

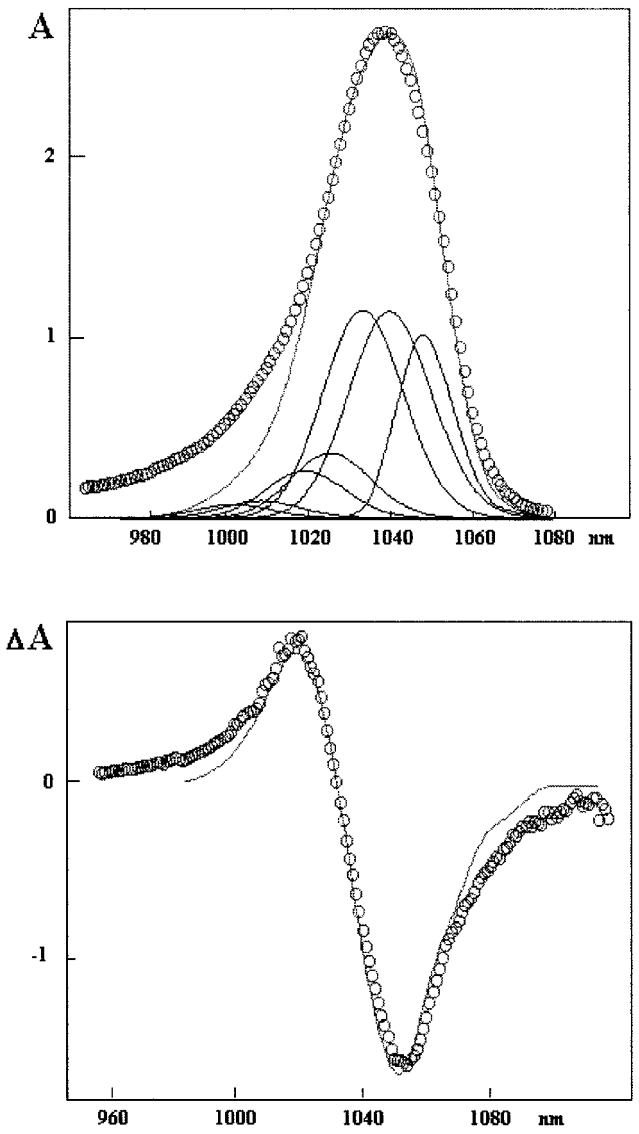

FIGURE 3 The same as in Fig. 2, but parameters are from fit no. 3: T = 77 K, N = 24, M_{12} = 400 cm^{-1}, γ_{1L} = 40 cm^{-1}, γ_{1H} = 182 cm^{-1}, γ_2 = 230 cm^{-1}, σ = 440 cm^{-1}, and the Stokes shift is 110 cm^{-1}.

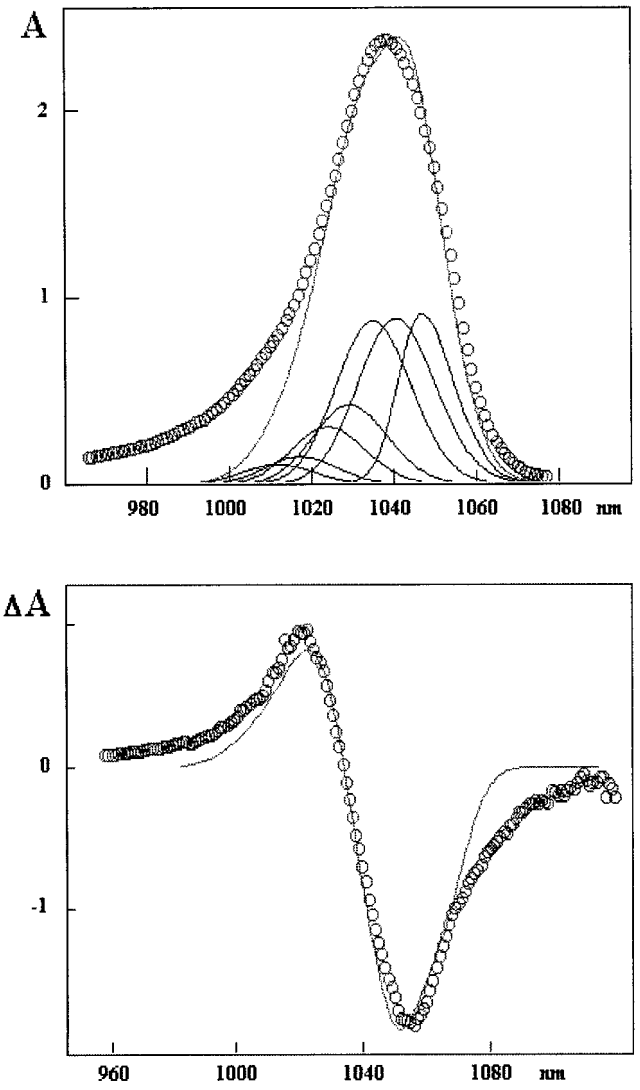

FIGURE 4 The same as in Fig. 2, but parameters are from fit no. 6: T = 77 K, N = 24, M_{12} = 260 cm^{-1}, γ_{1L} = 40 cm^{-1}, γ_{1H} = 166 cm^{-1}, γ_2 = 230 cm^{-1}, σ = 418 cm^{-1}, and the Stokes shift is 110 cm^{-1}.

limits of our model we are not able to explain the blue wing of absorption profile as well as the wings of the pump-probe spectra (blue wing of ESA and red wing of SE), which are most probably determined by the vibronic structure associated with each of the exciton levels.

It is important to note that the exciton model, used here to calculate the spectral features of LH1, is in good agreement with the earlier observation of spectral heterogeneity of LH1 of *Rps. viridis* (Monshouwer et al., 1995). The calculated maxima of the three lowest exciton levels at 77 K are very close to the 1049-, 1042-, and 1030-nm maxima observed in the second derivative of the absorption spectrum at low temperature (Monshouwer et al., 1995). Position, spectral width, and relative intensity of the lowest exciton level show good correlation with the same parameters of the B1045 spectral form (Monshouwer et al., 1995). The width of the B1045 band was determined as 12.4 nm at 4 K (Monshouwer et al., 1995), whereas the calculated width of the lowest exciton component is 15–18 nm at 77 K. The difference may easily be explained by the additional homogeneous broadening of the lowest level at 77 K (γ_{1L} = 40 cm^{-1}, or 4 nm in our model).

Notice that the spectral heterogeneity obtained here will be a common property of a spectrally disordered circular aggregate. The same (or, at least, similar) features may also be expected for the LH1 antenna of the BChl *a*–containing bacteria (recall that in our model the pigment arrangement is analogous to that of the BChl *a*–containing bacteria). However, no spectral heterogeneity was observed for the BChl *a*–containing species. For example, it was concluded that the long-wavelength side of the absorption spectrum for isolated LH1 complex of *Rb. sphaeroides* is dominated by inhomogeneous broadening (Van Mourik et al., 1992). In

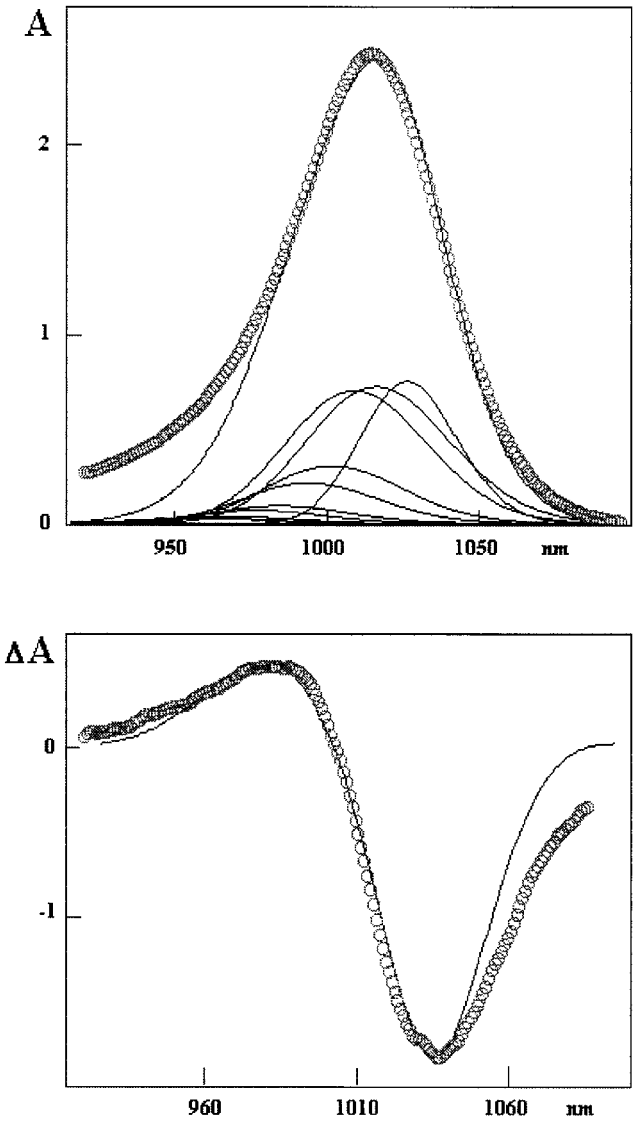

FIGURE 5 The same as in Fig. 2, but parameters are from fit no. 8: T = 300 K, $N = 24$, $M_{12} = 400\ \text{cm}^{-1}$, $\gamma_{1L} = 280\ \text{cm}^{-1}$, $\gamma_{1H} = 510\ \text{cm}^{-1}$, $\gamma_2 = 600\ \text{cm}^{-1}$, $\sigma = 550\ \text{cm}^{-1}$, and the Stokes shift is $140\ \text{cm}^{-1}$.

principle, the effect of heterogeneity may be masked by overlapping of spectral components. For example, the absorption peak of the lowest exciton level of a ring-like aggregate may be hidden under more intense absorption of higher levels. The possibility of resolving a fine structure of the overall spectrum may be strongly dependent on the positions, spectral widths, and shapes of individual exciton components. These parameters, determined by the static disorder and exciton-phonon coupling, are generally different for different species.

Delocalization of the exciton wave functions: participation ratio

Let us now consider the problem of delocalization of the exciton states of the spectrally disordered antenna. For a particular realization of the disorder, the kth one-exciton state is characterized by its energy E_k and wave function $|k\rangle$:

$$|\mathrm{k}\rangle = \sum_{n=1}^{N} c_n^k |n\rangle, \quad \sum_{n=1}^{N} |c_n^k|^2 = 1, \tag{1}$$

where $|n\rangle$ denotes the state in which molecule n is excited and all other molecules are in the ground state; c_n^k is the amplitude of the kth eigenfunction corresponding to the nth site. Quantitative information about the delocalization of the exciton wave functions can be obtained by using the participation ratio, defined as (Fidder et al., 1991)

$$L_k = \sum_{n=1}^{N} |c_n^k|^4. \tag{2}$$

The inverse participation ratio, $(L_k)^{-1}$, determines the delocalization length of kth exciton state. For example, for a localized state $c_n^k = \delta(n - n_0)$, and $(L_k)^{-1} = 1$, whereas for a completely delocalized wave function $c_n^k = N^{-1/2}$, and $(L_k)^{-1} = N$. Typically, the $(L_k)^{-1}$ values are different for different eigenstates. In this case an effective delocalization length can be defined as the thermally averaged inverse participation ratio (Meier et al., 1997c):

$$N_{\text{eff}} = \left\langle Z^{-1} \sum_k (L_k)^{-1} \exp(-E_k/k_B T) \right\rangle, \qquad Z = \sum_k \exp(-E_k/k_B T), \tag{3}$$

where k_B is the Boltzmann constant, T is temperature, and brackets indicate an average over realizations of the disorder. To obtain more detailed information about eigenstate-dependent delocalization degree, one can use the localization function (Fidder et al., 1991)

$$L(E) = \left\langle \sum_k L_k \delta(E - E_k) \right\rangle \Big/ \left\langle \sum_k \delta(E - E_k) \right\rangle. \tag{4}$$

which gives the degree of delocalization for the states at energy E. In numerical calculations the δ-function in Eq. 4 should be replaced by some function with small but nonzero width. We have used a Gaussian lineshape with a FWHM of $3\ \text{cm}^{-1}$. It is also convenient to plot L as a function of the wavelength λ instead of the energy E. The $L(\lambda)$ functions are shown in Figs. 6 and 7 for different interaction energies and intradimer asymmetries (parameters were taken from Table 2). They have a shape that is typical for a circular aggregate with a dimeric unit cell (for comparison, see the papers of Alden et al. (1997) and Liuolia et al. (1997)). An increase in L near the edges of the band is the result of diagonal disorder. The band consists of two subbands corresponding to the two Davydov components: the low-energy component is broader than the high-energy one, so that the boundary between them is shifted to the blue (one can see an increase in L at that point, i.e., at 900, 940, and 965 nm in the *top*, *middle*, and *bottom frames* of Fig. 6). In the

TABLE 2 The homogeneous linewidths (Γ_{1L}, Γ_{1H}, Γ_2), Stokes shift (S), and the site inhomogeneity values (σ) determined from the simultaneous fit of linear absorption and pump-probe spectra of the LH1 antenna of *Rhodopseudomonas viridis*

Fit no.	N	M_{12}	M_{23}	M_{13}	$E_1 - E_2$	σ	Γ_{1L}	Γ_{1H}	Γ_2	S
(a) Low-temperature (77 K) fit										
1	24	600	440	−78	0	495	40	191	230	105
2	24	600	440	−78	600	420	40	199	230	100
3	24	400	290	−52	0	440	40	182	230	110
4	32	400	290	−52	0	545	40	187	240	110
5	24	400	290	−52	600	385	40	195	230	105
6	24	260	190	−34	0	418	40	166	230	110
7	24	260	190	−34	600	370	40	172	230	110
(b) Room-temperature fit										
8	24	400	290	−52	0	550	280	510	600	140
9	32	400	290	−52	0	620	280	510	600	140

Fits 1–9 were obtained for $N = 24$ or 32 with different combinations of the interaction energies, M_{12}, M_{23}, M_{13} and the intradimer asymmetry parameter, $E_1 - E_2$. All values are given in cm^{-1}.

nearest-neighbor approximation ($M_{12} \neq 0$, $M_{23} \neq 0$, but $M_{13} = 0$) the Davydov components will be symmetrical, and this peak will be exactly in the middle of the band.

From the data shown in Figs. 6 and 7 we conclude that the individual exciton states are highly delocalized in the middle of the exciton band, i.e., in the blue edge of the absorption profile of LH1, but more localized near the absorption maximum (1040 and 1015 nm for low and room temperatures, respectively) and even more localized in the red wing. At low temperature (77 K) and for $N = 24$, the thermally averaged inverse participation ratio is equal to $N_{eff} = 9.1$, 7.4, and 5.4 for "high," "normal," and "low" interaction energies, respectively, with $E_1 - E_2 = 0$ or $N_{eff} = 8.7$, 6.5, and 3.8 with $E_1 - E_2 = 600\ cm^{-1}$ (see Table 3). At room temperature and for $N = 24$ we obtained $N_{eff} = 8.1$ for "normal" interaction energies and $E_1 - E_2 = 0$. (Notice that the thermally averaged inverse participation ratio increases with temperature because higher exciton states that are more delocalized start to contribute.) For $N = 32$ the N_{eff} value is slightly less than for $N = 24$ (Table 3) because of the higher disorder values required for the $N = 32$ fit. Using a fixed σ value, we will have approximately the same N_{eff} value for $N = 24$ and $N = 32$. It means that in our case the delocalization length is controlled mostly by the disorder (the exciton wave function does not "feel" the aggregate size). Notice that in the homogeneous limit the delocalization length is proportional to N (the inverse participation ratio for a homogeneous circular aggregate is equal to N for the lowest level and $2/3N$ for the higher ones). In general, the delocalization length increases with N and decreases with σ. The N values determine the delocalization length of the zero-order (homogeneous) wave functions, whereas the value of σ is responsible for mixing of these zero-order wave functions due to inhomogeneity, giving rise to more localized states.

Delocalization of the exciton wave packet: density matrix

Notice that the inverse participation ratio corresponds to a delocalization length for individual exciton states only. In reality one deals with some kind of superposition of exciton levels. For zero time delay (immediately after excitation) such a superposition may have been created because of the simultaneous excitation of several exciton levels. In the steady-state limit (for time delays longer than exciton relaxation) we will have a superposition of exciton states that are populated at thermal equilibrium. Evolution of the initially formed exciton wave packet (or selectively excited single exciton state) to the steady-state wave packet can be described by the density matrix in the site representation, $\rho_{m,n}(t)$, where n and m are molecular numbers (Meier et al., 1997a; Kühn and Mukamel, 1997; Kühn and Sundström, 1997). In the case of the disordered aggregate one should use the density matrix $\langle\rho_{m,n}(t)\rangle$ averaged over realizations of the disorder (everywhere below we omit these angular brackets). In the steady-state limit (with respect to exciton relaxation within the one-exciton manifold) the density matrix is given by (Meier et al., 1997c)

$$\rho_{m,n} = \sum_k c_m^k (c_n^k)^* \exp(-E_k/k_B T). \tag{5}$$

A three-dimensional view of the steady-state density matrixes at 77 K and 300 K are shown in Fig. 8. The disorder values and other parameters were taken from our fit nos. 3 and 8. The decay of the density matrix elements in the antidiagonal direction is determined by the delocalization length (or coherence length) of the exciton wave packet (Meier et al., 1997a,c; Kühn and Mukamel, 1997). In the literature there are different definitions for this length. Meier et al. (1997a) defined the coherent size, N_ρ, as the participation ratio of the density matrix:

$$N_\rho = \left(\sum_{m,n}\left|\rho_{m,n}\right|\right)^2 \Big/ \left(N\sum_{m,n}\left|\rho_{m,n}\right|^2\right). \tag{6}$$

In the absence of any coherence the density matrix is diagonal, $\rho_{m,n} = N^{-1}\delta(m - n)$, and $N_\rho = 1$. For a completely coherent exciton $\rho_{m,n} = N^{-1}$ and $N_\rho = N$. Another definition of the coherence length was proposed by Kühn and Sundström (1997). They introduced the coherence

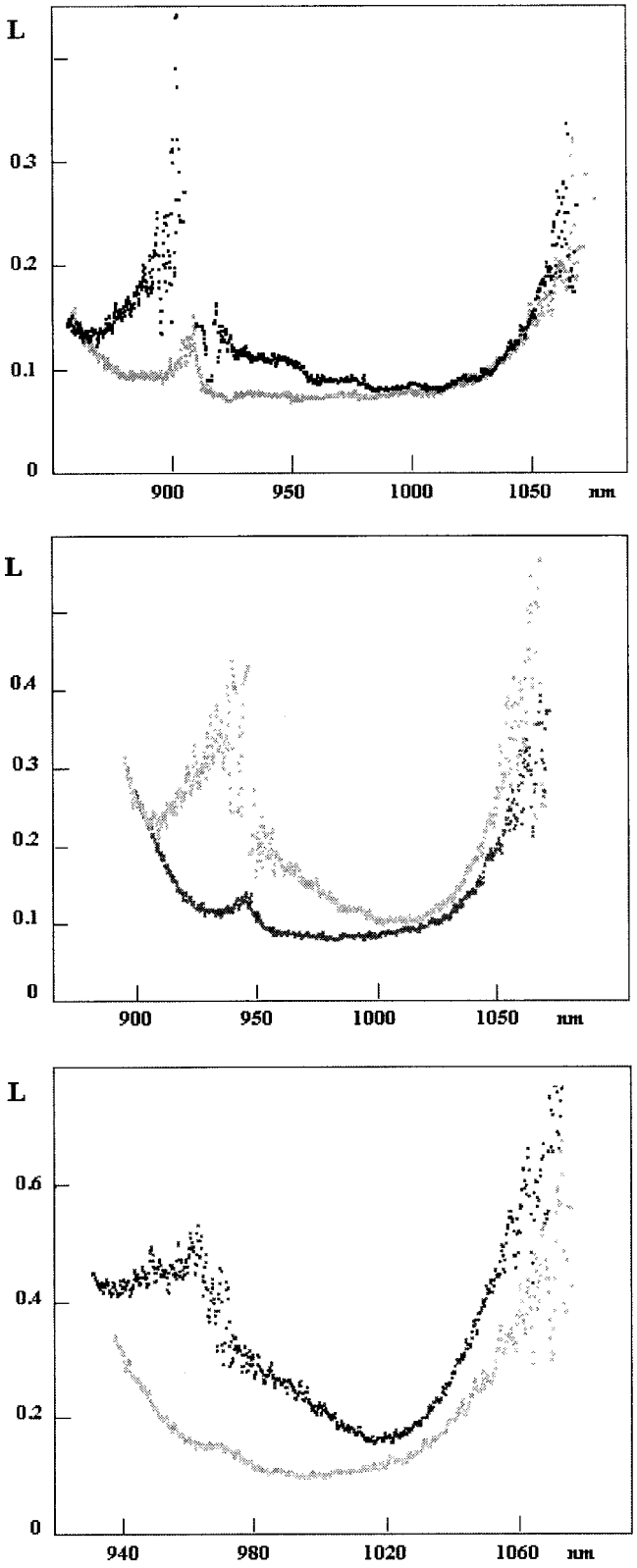

FIGURE 6 Localization function for the LH1 antenna with $N = 24$ at 77 K. (*Top*) $M_{12} = 600\ \text{cm}^{-1}$. (*Middle*) $M_{12} = 400\ \text{cm}^{-1}$. (*Bottom*) $M_{12} = 260\ \text{cm}^{-1}$. $E_1 - E_2 = 0$ (*lower curves*), $600\ \text{cm}^{-1}$ (*upper curves*). The σ values are taken from Table 2.

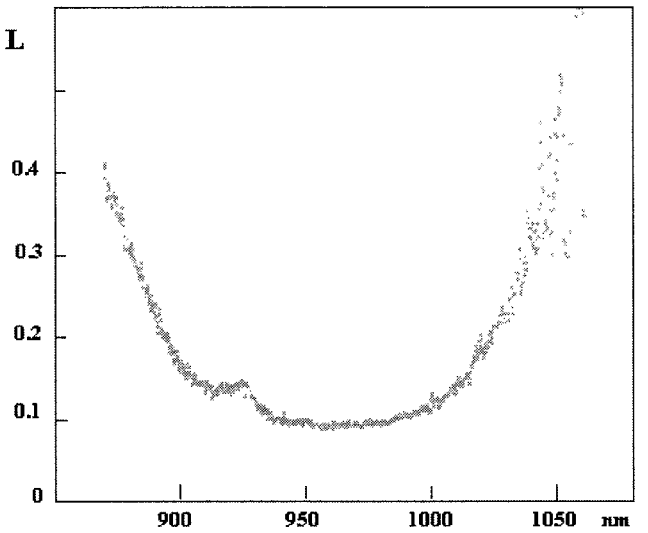

FIGURE 7 Localization function for the LH1 antenna at room temperature. $N = 24$, $M_{12} = 400\ \text{cm}^{-1}$, $\sigma = 550\ \text{cm}^{-1}$, $E_1 - E_2 = 0$.

function

$$C(n) = \sum_{m=1}^{N} |\rho_{m,m+n}|, \tag{7}$$

which is equal to the delta function, $C(n) = \delta(n)$, for a diagonal density matrix and $C(n) = 1$ for a completely coherent density matrix. In a real situation the steady-state coherence function $C(n)$ monotonically decays with n. Thus the coherence length, N_{coh}, can be defined as the FWHM of the $C(n)$ distribution (Kühn and Sundström, 1997). Typically, N_{coh} is significantly less than N_ρ, as can be seen from the density matrix plot obtained by Meier et al. (1997a). For example, for the B850 band of the LH2 antenna $N_{coh} = 8$, $N_\rho = 15$ at 4.2 K and $N_{coh} = 5$, $N_\rho = 7.9$ at 300 K (see figures 5 *c* and 7 *e* of Meier et al. (1997a)).

The steady-state coherence functions, $C(n)$, calculated with the parameters taken from the low-temperature and the room-temperature fits, are shown in Figs. 9 and 10, respectively. At low temperature the coherence length, N_{coh}, corresponds to 10, 8, and 6 molecules for "high," "normal," and "low" interaction energies, respectively, with $E_1 - E_2 = 0$ (Fig. 9, *top*) and to 10, 8, and 5 molecules, respectively, with $E_1 - E_2 = 600\ \text{cm}^{-1}$ (Fig. 9, *bottom*). These values are close to the inverse participation ratio, N_{eff}, so that the exciton wave packet length is approximately the same as the delocalization length for a single exciton level. Notice that in thermal equilibrium at 77 K only the lowest exciton level is populated (population of the second level for our parameters is $\sim$0.17–0.2), and consequently there is no significant superposition of levels.

In contrast, the N_{coh} value at room temperature corresponds to five molecules for "normal" interaction energies with $E_1 - E_2 = 0$ (Fig. 10). For "high" and "low" energies we obtain delocalization over six and four molecules, re-

TABLE 3 The exciton delocalization parameters for the LH1 antenna of *Rhodopseudomonas viridis*

Fit no.	N	M_{12}	$E_1 - E_2$	σ/M_{12}	N_{eff}	N_{coh}	$N_{\Delta A}$
(a) Low-temperature (77 K) fit							
1	24	600	0	0.825	9.1	10	11.2
2	24	600	600	0.700	8.7	10	11.0
3	24	400	0	1.100	7.4	8	10.1
4	32	400	0	1.363	6.3	8	9.8
5	24	400	600	0.963	6.5	8	8.4
6	24	260	0	1.607	5.4	6	7.8
7	24	260	600	1.423	3.8	5	5.4
(b) Room-temperature fit							
8	24	400	0	1.375	8.1	5	6.7
9	32	400	0	1.550	7.7	5	6.5

The thermally averaged inverse participation ratio, N_{eff}, coherence length, N_{coh}, and photobleaching length, $N_{\Delta A}$ (relative amplitude of the bleaching peak of difference absorption) are shown for different values of N, M_{12}, $E_1 - E_2$, σ/M_{12}, taken from Table 2, fits 1–9.

spectively (data not shown). This is significantly less than N_{eff} because of the strong contribution of the lowest four or five levels that are populated in the steady-state limit to the superposition. We also found that the N_{coh} value does not depend on the aggregate size, N, both for low and room temperature (Table 3).

Notice that the delocalization length can also be obtained by calculating the actual squared wave function of the exciton states (Monshouwer et al., 1997). Direct averaging of the squared wave function over disorder and over states will give uniform distribution because the maximum of the wave function changes its position from state to state and from one realization of disorder to another. To obtain the averaged shape of the wave function some artificial shift of its position for each state and in each realization should be introduced. Similarly, the actual shape of the exciton wave packet can be calculated as a superposition of the exciton wave functions (Dracheva et al., 1997). In this case one should average the squared superposition $f(n) = |a_1 c_n^1 + a_2 c_n^2 + \ldots|$, where $|a_k|^2 = Z^{-1} \exp(-E_k/k_B T)$ in the steady-state limit. The temperature-dependent wave packet shapes $f(n)$ were calculated with artificially fixed phases of the a_k coefficients (Dracheva et al., 1997). Interestingly, this simplified calculation gave approximately the same value for the coherence length (about five BChls at room temperature for the LH2 antenna of *Rps. acidophila*) as the more advanced density matrix approach used in this paper.

Initially formed exciton wave packet

Finally, we have calculated the pump-probe spectrum that is formed immediately after short-wavelength excitation (at 1017 nm) at low temperature. The calculation is the same as the calculation of the steady-state spectra, but in this case we used the nonequilibrium populations of one-exciton states created by the pump pulse instead of the steady-state ones. These initially created populations depend on the overlap of the pump spectrum and the spectral lineshapes of the various exciton components. It is reasonable to suppose that the pump pulse (100 fs duration) is not short enough to create a coherence between the one-exciton states. On the other hand, we neglected for simplicity the excitonic and vibronic relaxation during the pump pulse as well as the contributions to the pump-probe signal due to the overlap of pump and probe pulses (coherent artefact). The thus calculated pump-probe spectrum at short time delay is shown in Fig. 11, together with the steady-state spectrum. The experimental spectra correspond to 60-fs and 1.1-ps delays. Both calculated and experimental steady-state spectra demonstrate a 10-nm red shift with respect to the initially created spectra. The time constant of this shift is ~130 fs, according to the analysis of the experimental kinetics (Monshouwer et al., 1998). Notice that within the context of our model the 1017-nm pump corresponds to the excitation of higher exciton levels, so that the time-dependent red shift is a result of energy relaxation to the lowest exciton level of the antenna. Comparison of measured and calculated spectra (Fig. 11) allows us to estimate the relaxation time of these higher exciton levels as 130 fs.

The initial coherence function is shown in Fig. 12 together with the steady-state one. The initially created exciton wave packet is delocalized over five molecules, but some part of the excitation is delocalized over the whole ring. Such a nonuniform delocalization is a result of the superposition of several exciton levels that are simultaneously excited by the pump pulse. After relaxation to the steady-state distribution, in which only the lowest exciton level is populated, we find that the exciton wave packet is delocalized over eight molecules.

Alternative models of the core antenna

Our model of the core antenna is based on the assumption that the pigment arrangement in *Rps. viridis* is approximately the same as in the LH2 complex of the BChl *a*–containing bacteria. When the geometry of the complex is fixed, the only thing we have to know for our calculations is the Hamiltonian of the system. The latter contains the unperturbed diagonal energies E_1, E_2 and interaction energies M_{12}, M_{23}, and M_{13}. If we have any set of these parameters, then all spectroscopic parameters (linewidths, static disorder value, Stokes shift) as well as dynamical properties

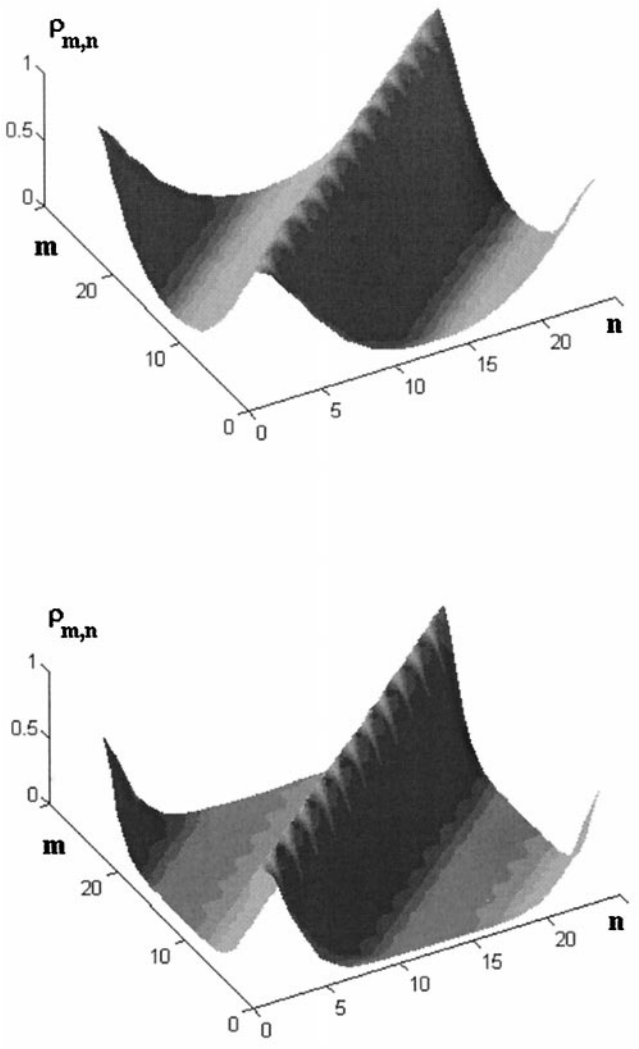

FIGURE 8 Three-dimensional view of the steady-state density matrix, $\rho_{m,n}$, at 77 K (*top*) and room temperature (*bottom*). Parameters from fit nos. 3 and 8, i.e., $N = 24$, $M_{12} = 400\ cm^{-1}$, $E_1 - E_2 = 0$, $\sigma = 440$, and 550 cm^{-1}, for 77 K and 300 K, respectively. *x* and *y* coordinates correspond to the molecular numbers, *n* and *m*.

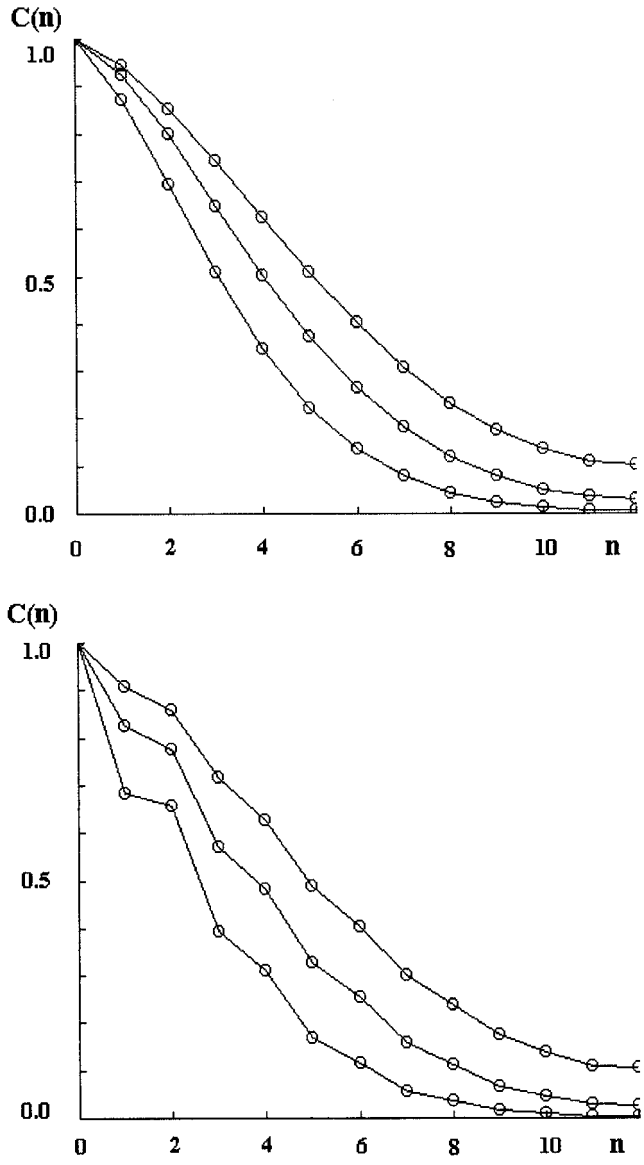

FIGURE 9 The steady-state low-temperature coherence function. $N = 24$; $E_1 - E_2 = 0$ (*top*) and 600 cm^{-1} (*bottom*). Different curves correspond to the "high," "normal," and "low" interaction energies (*from top to bottom*). Parameters are taken from Table 2, fit nos. 1–3 and 5–7.

(delocalization length, amplitude of time-dependent red shift of transient absorption) can more or less be precisely determined from a simultaneous fit of the linear and nonlinear spectra. We have shown this to be the case for different sets of diagonal and interaction energies. The absolute values of both diagonal and interaction energies depend on microscopic factors and typically they are not well known. But the relative values of interaction energies can be estimated from the geometry of the complex, so that we may predict how changes in the geometry will affect the exciton structure and optical spectra of the antenna. In this section we analyze some alternative models for the core antenna of *Rps. viridis* with a pigment organization different from that of LH2 complex of the BChl *a*–containing bacteria.

Recent 10-Å-resolution studies of reaction center–LH1 complex of *Rps. viridis* (Ikedayamasaki et al., 1998) suggested that the pigments in the antenna are arranged in a ringlike structure at approximately equal distances from the geometrical center of the complex. However, the data gave no information about the symmetry of the BChl arrangement in the ring. In our model we consider a circular aggregate of 24–32 BChl *b* molecules with either C_{12} or C_{16} symmetry (the elementary unit cell contains two BChl *b* molecules, bound to the α-β heterodimer). The distances between BChls in a dimeric unit and between nearest BChls from different units are $r_{12} = 0.87$ nm and $r_{23} = 0.97$ nm, respectively, as in the LH2 antenna from *Rps. acidophila* (McDermott et al., 1995). As a first alternative we have considered the same model but with larger interdimer distances, i.e., varying r_{23} from 0.97 nm to 2.0 nm with

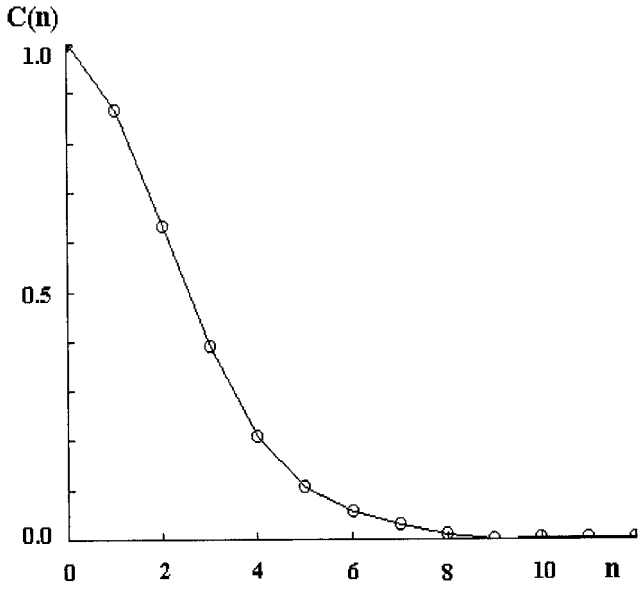

FIGURE 10 The steady-state room-temperature coherence function calculated for "normal" interaction energies, $N = 24$, $E_1 - E_2 = 0$. Parameters are taken from Table 2, fit no. 8.

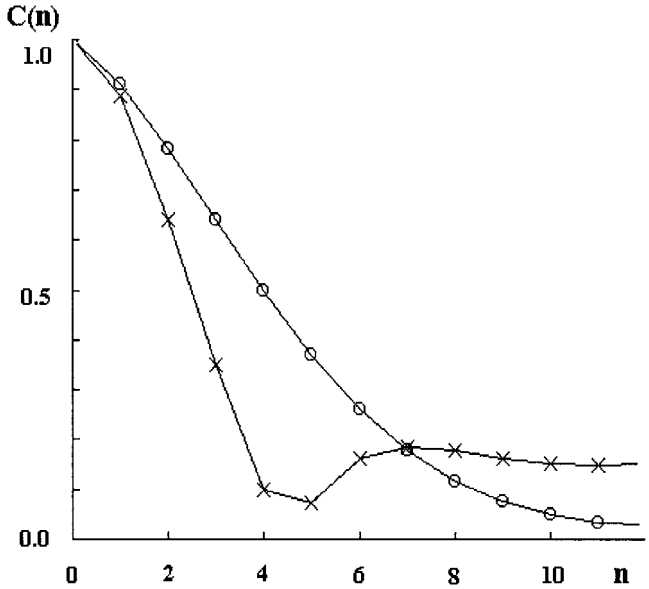

FIGURE 12 Coherence function calculated for short delay (×) and for steady-state limit (○). Parameters are the same as in Fig. 11.

corresponding scaling of the interaction energies M_{23} and M_{13}. The intradimer parameters were fixed ($r_{12} = 0.87$ nm, $M_{12} = 400$ cm^{-1}). We found that for $r_{23} < 1.3$ nm it is possible to obtain a reasonable fit of linear and nonlinear spectra, but for larger r_{23} it is impossible to fit the pump-probe spectrum. The calculated difference absorption for large interdimer distance shows a very broad ESA band with an increase in the splitting between positive and negative peaks. These features indicate that the exciton becomes more localized (Meier et al., 1997a). The distance of $r_{23} = 1.3$ nm corresponds to $M_{23} = 160$ cm^{-1} instead of 290 cm^{-1} at $r_{23} = 0.97$ nm. The delocalization parameters at $r_{23} = 1.3$ nm are $N_{\text{eff}} = 6.8$ and $N_{\text{coh}} = 4.0$ (at room temperature) instead of $N_{\text{eff}} = 8.1$ and $N_{\text{coh}} = 5.0$ for $r_{23} = 0.97$ nm. We conclude that our model is not very sensitive to a possible asymmetry in the pigment-pigment distances in the LH1 complex. For the geometry with $r_{12} = 0.87$ nm and $r_{23} = 1.3$ nm, we are still able to explain the experimental spectra, and we predict that the dynamical properties (delocalization lengths) in this case are not much different from those for the symmetrical geometry. It is clear that we will get the same result for similar types of asymmetry that increase the difference between pigment-pigment interaction energies (for example, orientational asymmetry). We also cannot rule out the possible existence of some specific geometry that will increase the interaction energies in the LH1 complex of *Rps. viridis* with respect to LH1 and LH2 complexes of the BChl *a*–containing species. Of course, such an increased interaction will help us to explain the anomalously large red shift of the absorption band of *Rps. viridis* as well as its more pronounced heterogeneity, as compared with the LH1 antennae of BChl *a*–containing bacteria. In this case we also should expect a higher degree of delocalization in the *Rps. viridis* antenna.

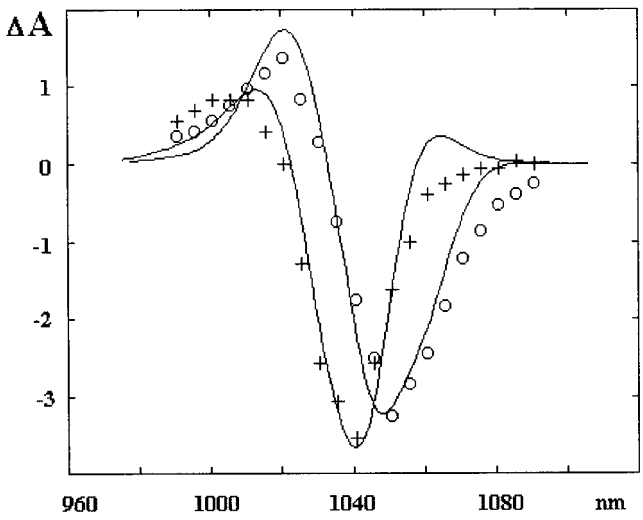

FIGURE 11 The low-temperature pump-probe spectra at short-wavelength (1017 nm) excitation. Experimental points correspond to a 60-fs delay (+) and a 1.1-ps delay (○). Calculated spectra for short delay and for steady-state limit (*solid lines*) were obtained using the same parameters as in Fig. 3 (fit no. 3).

Another alternative arrangement of pigments in a ring may have the form of weakly interacting quasilinear aggregates of BChls. For example, for $N = 24$ one can imagine three clusters of eight BChls or four clusters of six BChls; for $N = 32$ it can be four clusters of eight molecules, and so on. However, a calculation showed that for all of these models the largest part of the dipole strength is concentrated in the lowest exciton level. This means that the second derivative of the absorption spectrum will have one intense peak, the low-temperature fluorescence spectrum will be as

broad as the absorption spectrum, the CD spectrum will have the zero-crossing point shifted to the blue from the absorption maximum, etc., in contradiction to the experimental data (Monshouwer et al., 1995). To obtain the correct exciton structure one should suppose an excitonic coupling within a much larger fragment of the ring (more than a half of the ring). On the other hand, if we suppose that the LH1 ring is not closed, but one or two dimeric subunits are removed, the exciton structure of such an antenna will be approximately the same as for the closed ring (this is valid only in the case of a disordered ring when the dipole strength of the lowest level is essentially more than the monomeric dipole strength).

DISCUSSION

Determination of the delocalization length from spectroscopic data

The main results of our calculations are summarized in Table 3, where we show the parameters that characterize the excitonic interactions in the LH1 antenna of *Rps. viridis* (interaction energy, M_{12}, intradimer asymmetry, $E_1 - E_2$, and the dimensionless disorder value, σ/M_{12}) together with the different coherence sizes of the exciton. The degree of exciton delocalization can be characterized by two parameters: 1) the delocalization length for the individual exciton states, N_{eff}, defined as the inverse participation ratio of the exciton wave function; 2) the coherence length of the exciton wave packet, $N_{\rho\mathrm{r}}$, defined as the inverse participation ratio of the density matrix, or the coherence length, N_{coh}, defined as the decay length (FWHM) of the density matrix in the antidiagonal direction. In nonlinear spectroscopic experiments other parameters appear, such as the superradiance length, N_{S} (Meier et al., 1997a,c). In the case of nonlinear absorption studies it is possible to introduce the bleaching length, $N_{\Delta\mathrm{DA}}$, defined as the amplitude of the negative ("bleaching") peak of the difference absorption, normalized to the bleaching amplitude of the BChl monomer. Of course, such a $N_{\Delta\mathrm{DA}}$ value will depend on the parameters of the reference system, i.e., of the BChl monomer. In our calculation we have assumed that the homogeneous width and the Stokes shift for this monomer are the same as those for the lowest exciton level of the antenna, i.e., $\gamma_{1\mathrm{L}}$ and S, and furthermore that the inhomogeneous width of the monomeric spectrum is equal to the site inhomogeneity of the antenna, σ. We also assumed that the excitation of the monomer by the pump pulse is nonselective. Notice that such a monomer is not real, but rather is some model object, so that the $N_{\Delta\mathrm{DA}}$ values in Table 3 are actually measured in some relative units.

The most important manifestation of exciton delocalization is the increase in amplitude of the PB, SE, and ESA components of the difference absorption, which are proportional to the dipole strength of the one- and two-exciton transitions, which, in turn, are proportional to the delocalization length of the corresponding exciton states. That is why the $N_{\Delta\mathrm{DA}}$ value is directly connected to the N_{eff} and N_{coh} values. On the other hand, $N_{\Delta\mathrm{DA}}$ is essentially different from these two, because this number is also determined by the spectral overlap of the exciton transitions within the PB, SE, and ESA spectra, as well as by the overlap and partial compensation of the negative PB/SE and positive ESA components (Mukamel, 1995; Dracheva et al., 1997).

Let us now discuss the relationship between the different coherence sizes and the parameters M_{12}, $E_1 - E_2$, and σ/M_{12}, which describe the excitonic interactions in the spectrally disordered antenna. Notice that these parameters cannot be directly estimated from any experiment because they are connected with the microscopic properties of the pigment-protein complex. On the other hand, they also cannot be precisely determined from a fit of the spectroscopic data. For example, we have obtained approximately the same relative positions of the exciton components and the same shapes of the linear and nonlinear absorption for essentially different values of the interaction energies. In general, a decrease in the interaction energy results in a proportional decrease in the interlevel splitting. But in a disordered aggregate this effect is compensated for by an additional increase in the splitting due to site inhomogeneity (if σ is comparable to M_{12}, then the splitting will be proportional to the σ/M_{12} ratio). Consequently, the combined action of these two factors gives rise to approximately the same interlevel distance if we change the interaction energy without significantly altering the disorder value. This allows us to obtain a satisfactory fit of the linear and nonlinear spectral shapes for different M_{12} and, therefore, different σ/M_{12} values. On the other hand, the dimensionless disorder value, σ/M_{12}, is responsible for the destruction of delocalized exciton states. An increase in σ/M_{12} results in a proportional decrease in N_{eff} and N_{coh} (Table 3). This means that we are not able to determine precisely the exciton delocalization degree from the fit of spectral shapes only. Such a fit allows us to determine just the limits of delocalization parameters. For example, the exciton wave packet length according to our estimation corresponds to 5–10 molecules at low temperature and 4–6 at room temperature. On the other hand, the variations in the $N_{\Delta\mathrm{DA}}$ value are closely correlated with variations in N_{eff} and N_{coh} (Table 3). This means that the amplitude of the difference absorption contains information that can be used for a more precise estimate of the delocalization parameters. Let us now discuss some experiments that may allow the precise measurement of the value of $N_{\Delta\mathrm{DA}}$ in antenna complexes of purple bacteria.

1. In the case of B800–850 (LH2) complexes it is possible to compare bleaching values of the B850 ring and of the B800 monomer (Kennis et al., 1996). Similarly, for the B808–866 complex from the green bacterium *Chloroflexus aurantiacus*, the bleaching value of the B866 band can be compared with that of the monomeric B808 band (Novoderezhkin et al., 1998). In such experiments the monomeric bleaching peak can be significantly narrowed because of selective interaction of the pump pulse with the inhomoge-

neously broadened B800(808) band. This will reduce the ratio of the bleaching values for the B850(866) and B800(808) bands. The experimental value of this ratio is ~3 for both B800–850 (Kennis et al., 1996) and B808–866 complexes (Novoderezhkin et al., 1998) at room temperature.

2. It is possible to compare the difference absorption amplitudes for the LH1 or LH2 antenna and for the isolated B820 dimeric subunit (Monshouwer, 1998; Novoderezhkin et al., manuscript submitted for publication). The $N_{\Delta DA}$ values will be reduced two times if we use the dimeric unit as a reference system instead of the monomer. The experimentally observed ratio of the amplitude of PB for LH2 of *Rb. sphaeroides* compared with the B820 subunit is 3.3 at room temperature (Monshouwer, 1998).

3. In the case of the core (LH1) antenna it is possible to compare the initial amplitude of the difference absorption in the antenna due to its excitation with the long-lived bleaching of the BChl dimer (special pair) of the reaction center due to its oxidation (Novoderezhkin and Razjivin, 1993, 1995b; Kennis et al., 1994; Xiao et al., 1994). For a correct interpretation of the experimental data one should know the dipole strength and the linewidth of the lowest exciton level of a special pair, as well as the quantum yield of energy trapping by the reaction center. Moreover, these experiments should be performed under truly nonannihilating conditions, which are difficult to achieve in these highly connected systems.

Notice that at room temperature the PB, SE, and ESA components of the spectrum are strongly overlapping. At low temperature it is possible to extract the SE component from the difference absorption of the B850 and B800 bands (Kennis et al., 1997). From the ratio of their integrated intensities Kennis et al. (1997) estimated the dipole strength of the lowest exciton level as 2.3–3.4. From the low-temperature fluorescence data this value was estimated as 2.8 and 3.8 for the LH2 and LH1 antenna, respectively (Monshouwer et al., 1997). Our model of the LH1 antenna of *Rps. viridis* gave 3.4–4.1 for $N = 24$ and 4.7–5.5 for $N = 32$. Notice that the dipole strength of the lowest exciton level determines the low-temperature superradiance length, N_S. The relation between N_S and N_ρ was studied by Meier et al. (1997c).

Electronic and vibrational dephasing

In the model used so far to fit the spectral data, we did not take into account the coupling of the exciton with intra- and intermolecular vibrational modes as well as with phonon modes of the thermal bath. The spectral line broadening was simply described by introducing symmetrical Gaussian lineshapes. In more realistic models the collective nuclear degrees of freedom should be explicitly taken into account. Time-resolved pump-probe studies of the LH1 antenna of *Rps. viridis* have shown that electronic excitations are coupled with two vibrational modes of 65 and 103 cm^{-1} (Monshouwer et al., 1998). The corresponding oscillatory features observed in the pump-probe kinetics have a large amplitude and a decay time of ~700–800 fs, which is much larger than the characteristic time of electronic energy transfer and dephasing (100–150 fs). Very similar observations were made earlier for the LH1 antenna of *Rb. sphaeroides* (Bradforth et al., 1995; Chachisvilis and Sundström, 1996). The microscopic origin of electronic and vibrational dephasing in molecular systems coupled to a thermal bath implies that the interaction of the bath with the molecule is only weakly dependent on the nuclear coordinates but strongly depends on the electronic state of the system (Mukamel, 1995). This is why bath-induced vibrational dephasing is much slower than pure dephasing and relaxation between different electronic (excitonic) levels. However, in a large molecular aggregate vibrational dephasing may be strongly influenced by the electronic energy transfer dynamics.

In general, electronic excitation is followed by some changes in the equilibrium position of the nuclear coordinates associated with the relevant vibrational modes. Nonlinear interaction of the exciton with these deformations may significantly influence the exciton dynamics.

In the limit of weak exciton-phonon coupling the deformations are uniform, and they do not destroy the delocalized exciton states (Davydov, 1971). In this case the pump pulse can produce a delocalized exciton state or exciton wave packet together with coherent vibrations of all of the molecules in the aggregate. Fast dephasing and relaxation of exciton states are followed by a dynamic red shift of the pump-probe spectra and the pump-probe anisotropy decay, but do not influence the coherent nuclear motion and do not shorten the vibrational dephasing.

In the opposite limit of very strong exciton-phonon coupling ($S \gg 1$, where S is the Huang-Rhys factor; Grover and Silbey, 1970; Fischer and Rice, 1970), the exciton is self-trapped at one unit cell (e.g., the dimer). In this case both the anisotropy decay and the decay of local vibrations can be explained only by noncoherent "hopping" of localized excitation. To explain a slow decay of vibrations during the hopping process, one should suppose some form of the vibrational coherence transfer via noncoherent exciton motion (Bradforth et al., 1995; Monshouwer et al., 1998).

In the intermediate case ($S \approx 1$) the nonlinear interaction of the exciton with local deformations results in the formation of a polaron (or "dressed" exciton) delocalized over some area that can be significantly less than the whole aggregate size (Davydov, 1971; Agranovich and Galanin, 1982; Grover and Silbey, 1970; Fischer and Rice, 1970). The exciton bandwidth is reduced by a factor of $\exp(-S)$. The distribution of vibrational amplitudes is essentially nonuniform, reflecting the excitation density distribution. In this case there are three time scales: 1) the time of vibrational dephasing due to coupling with the bath phonons; 2) the characteristic time of noncoherent motion of the delocalized polaron, which is much greater than the hopping time of localized excitation; and 3) the time of electronic relaxation within a renormalized exciton band. It is reason-

able to suppose that the decay of the vibrational coherence will be controlled by the shorter of the first two time scales 1) and 2), whereas the fast component of the anisotropy decay can be explained by the third time, 3).

Delocalization length and exciton-phonon coupling

In this paper we have estimated the degree of exciton delocalization in the antenna, taking into account the static disorder but neglecting the effects of dynamic disorder due to fast nuclear dynamics in pigment-protein complexes. The role of nuclear degrees of freedom depends on their coupling with electronic excitations. In the case of weak exciton-phonon coupling the dynamic disorder may influence the kinetics of exciton relaxation, but the steady-state delocalization length does not depend on the nature of phonons and exciton-phonon coupling strength, being determined by the static disorder only (Meier et al., 1997c). Strong exciton-phonon coupling may give rise to further reduction of the disorder-induced localization length due to polaron formation (Meier et al., 1997c). This means that our estimations of the coherence size are valid in the weak-coupling limit, but they should be corrected in the strong-coupling limit if N_{eff} and N_{coh} are larger than the polaron-induced length, N_{ph}. We will revisit this problem in the future, using the theory of fluorescence, photon echo, and pump-probe spectroscopies of the photosynthetic antenna complexes with static disorder and strong exciton-phonon coupling that has recently been developed (Meier et al., 1997b,c; Zhang et al., 1998a,b).

VN was supported by a visitors grant from the Dutch Foundation of Scientific Research (NWO) and by the Russian Foundation for Basic Research, grant 97-04-49842. The research was supported by the Foundation of Earth and Life Sciences (ALW), part of the Dutch Foundation of Scientific Research and the Human Frontiers in Science Program, grant 1932802.

REFERENCES

Agranovich, V. M., and M. D. Galanin. 1982. Electronic Excitation Energy Transfer in Condensed Matter. North-Holland, Amsterdam.

Alden, R. G., E. Johnson, V. Nagarajan, W. W. Parson, C. J. Law, and R. J. Cogdell. 1997. Calculation of spectroscopic properties of the LH2 bacteriochlorophyll-protein antenna complex of *Rhodopseudomonas acidophila. J. Phys. Chem. B.* 101:4667–4680.

Bradforth, S. E., R. Jimenez, F. van Mourik, R. van Grondelle, and G. R. Fleming. 1995. Excitation transfer in the core light-harvesting complex (LH-1) of *Rhodobacter sphaeroides:* an ultrafast fluorescence depolarization and annihilation study. *J. Phys. Chem.* 99:16179–16191.

Chachisvilis, M., and V. Sundström. 1996. Femtosecond vibrational dynamics and relaxation in the core light-harvesting complex of photosynthetic purple bacteria. *Chem. Phys. Lett.* 261:165–174.

Davydov, A. S. 1971. Theory of Molecular Excitons. Plenum Press, New York.

Dracheva, T. V., V. I. Novoderezhkin, and A. P. Razjivin. 1996. Exciton delocalization in the antenna of purple bacteria: exciton spectra calculation using x-ray data and experimental site inhomogeneity. *FEBS Lett.* 378:81–84.

Dracheva, T. V., V. I. Novoderezhkin, and A. P. Razjivin. 1997. Exciton delocalization in the light-harvesting LH2 complex of photosynthetic purple bacteria. *Photochem. Photobiol.* 66:141–146.

Fidder, H., J. Knoester, and D. A. Wiersma. 1991. Optical properties of disordered molecular aggregates: a numerical study. *J. Chem. Phys.* 95:7880–7890.

Fischer, S., and S. A. Rice. 1970. Frenkel excitons in a vibrating molecular crystal. *J. Chem. Phys.* 52:2089–2098.

Grover, M. K., and R. Silbey. 1970. Exciton-phonon interaction in molecular crystals. *J. Chem. Phys.* 52:2099–2108.

Jimenez, R., S. N. Dikshit, S. E. Bradforth, and G. R. Fleming. 1996. Electronic excitation transfer in the LH2 complex of *Rhodobacter sphaeroides. J. Phys. Chem.* 100:6825–6834.

Hu, X., T. Ritz, A. Damjanovic, and K. Schulten. 1997. Pigment organization and transfer of electronic excitation in the photosynthetic unit of purple bacteria. *J. Phys. Chem. B.* 101:3854–3871.

Ikedayamasaki, I., T. Odahara, K. Mitsuoka, Y. Fujiyoshi, and K. Murata. 1998. Projection map of the reaction center-light harvesting 1 complex from *Rhodopseudomonas viridis* at 10-angstrom resolution. *FEBS Lett.* 425:505–508.

Karrasch, S., P. A. Bullough, and R. Ghosh. 1995. The 8.5 Å projection map of the light-harvesting complex I from *Rhodospirillum rubrum* reveals a ring composed of 16 subunits. *EMBO J.* 14–4:631–638.

Kennis, J. T. M., T. J. Aartsma, and J. Amesz. 1994. Energy trapping in the purple bacteria *Chromatium vinosum* and *Chromatium tepidum. Biochim. Biophys. Acta.* 1188:278–286.

Kennis, J. T. M., A. M. Streltsov, T. J. Aartsma, T. Nozava, and J. Amesz. 1996. Energy transfer and exciton coupling in isolated B800–850 complexes of the photosynthetic purple sulfur bacterium *Chromatium tepidum*. The effect of structural symmetry on bacteriochlorophyll excited states. *J. Phys. Chem.* 100:2438–2442.

Kennis, J. T. M., A. M. Streltsov, H. Permentier, T. J. Aartsma, and J. Amesz. 1997. Exciton coherence and energy transfer in the LH2 complex of *Rhodopseudomonas acidophila* at low temperature. *J. Phys. Chem. B.* 101:8369–8374.

Koepke, J., X. Hu, C. Muenke, K. Schulten, and H. Michel. 1996. The crystal structure of the light-harvesting complex II (B800–850) from *Rhodospirillum molischianum. Structure.* 4:581–597.

Koolhaas, M. H. C., R. N. Frese, G. J. S. Fowler, T. S. Bibby, S. Georgakopoulou, G. Van der Zwan, C. N. Hunter, and R. Van Grondelle. 1998. Identification of the upper exciton component of the B850 bacteriochlorophylls of the LH2 antenna complex, using a B800-free mutant of *Rhodobacter sphaeroides. Biochemistry*. 37:4693–4698.

Kühn, O., and S. Mukamel. 1997. Probing the two-exciton manifold of light-harvesting antenna complexes using femtosecond four-wave mixing. *J. Phys. Chem. B.* 101:809–816.

Kühn, O., and V. Sundström. 1997. Pump-probe spectroscopy of dissipative energy transfer dynamics in photosynthetic antenna complexes: a density matrix approach. *J. Chem. Phys.* 107:4154–4164.

Leupold, D., H. Stiel, K. Teuchner, F. Novak, W. Sandner, B. Ucker, and H. Scheer. 1996. Size enhancement of transition dipoles to one- and two-exciton bands in a photosynthetic antenna. *Phys. Rev. Lett.* 77: 4675–4678.

Liuolia, V., L. Valkunas, and R. van Grondelle. 1997. Excitons in chains of dimers. *J. Phys. Chem. B.* 101:7343–7349.

McDermott, G., S. M. Prince, A. A. Freer, A. M. Hawthornthwaite-Lawless, M. Z. Papiz, R. J. Cogdell, and N. W. Isaacs. 1995. Crystal structure of an integral membrane light-harvesting complex from photosynthetic bacteria. *Nature.* 374:517–521.

Meier, T., V. Chernyak, and S. Mukamel. 1997a. Multiple exciton coherence sizes in photosynthetic antenna complexes viewed by pump-probe spectroscopy. *J. Phys. Chem. B.* 101:7332–7342.

Meier, T., V. Chernyak, and S. Mukamel. 1997b. Femtosecond photon echoes in molecular aggregates. *J. Chem. Phys.* 107:8759–8774.

Meier, T., Y. Zhao, V. Chernyak, and S. Mukamel. 1997c. Polarons, localization, and excitonic coherence in superradiance of biological antenna complexes. *J. Chem. Phys.* 107:3876–3893.

Miller, K. R. 1982. Three-dimensional structure of a photosynthetic membrane. *Nature.* 300:53–55.

Monshouwer, R. 1998. The nature and dynamics of excitations in photosynthetic light-harvesting. Ph.D. thesis. Vrije Universiteit Amsterdam, the Netherlands.

Monshouwer, R., M. Abrahamsson, F. van Mourik, and R. van Grondelle. 1997. Superradiance and exciton delocalization in bacterial photosynthetic light-harvesting systems. *J. Phys. Chem. B.* 101:7241–7248.

Monshouwer, R., A. Baltuška, F. van Mourik, and R. van Grondelle. 1998. Time-resolved absorption difference spectroscopy of the LH1 antenna of *Rhodopseudomonas viridis. J. Phys. Chem. A.* 102:4360–4371.

Monshouwer, R., R. W. Visschers, F. van Mourik, A. Freiberg, and R. van Grondelle. 1995. Low-temperature absorption and site-selected fluorescence of the light-harvesting antenna of *Rhodopseudomonas viridis*. Evidence for heterogeneity. *Biochim. Biophys. Acta.* 1229:373–380.

Mukamel, S. 1995. Principles of Nonlinear Optical Spectroscopy. Oxford University Press, New York and Oxford.

Novoderezhkin, V. I., and A. P. Razjivin. 1993. Excitonic interactions in the light-harvesting antenna of photosynthetic purple bacteria and their influence on picosecond absorbance difference spectra. *FEBS Lett.* 330:5–7.

Novoderezhkin, V. I., and A. P. Razjivin. 1995a. Exciton dynamics in circular aggregates: application to antenna of photosynthetic purple bacteria. *Biophys. J.* 68:1089–1100.

Novoderezhkin, V. I., and A. P. Razjivin. 1995b. Excitation delocalizaiton over the whole core antenna of photosynthetic purple bacteria evidenced by non-linear pump-probe spectroscopy. *FEBS Lett.* 368:370–372.

Novoderezhkin, V. I., A. S. Taisova, Z. G. Fetisova, R. E. Blankenship, S. Savikhin, D. R. Buck, and W. S. Struve. 1998. Energy transfer in the B808–866 antenna from the green bacterium *Chloroflexus aurantiacus. Biophys. J.* 74:2069–2075.

Pullerits, T., M. Chachisvilis, and V. Sundström. 1996. Exciton delocalization length in the B850 antenna of *Rhodobacter sphaeroides. J. Phys. Chem.* 100:10787–10792.

Sauer, K., R. J. Cogdell, S. M. Prince, A. Freer, N. W. Isaacs, and H. Scheer. 1996. Structure-based calculations of the optical spectra of the LH2 bacteriochlorophyll-protein complex from *Rhodopseudomonas acidophila. Photochem. Photobiol.* 64:564–576.

Stark, W., W. Kühlbrandt, I. Wildhaber, E. Wehrli, and K. Muhlethaler. 1984. The structure of the photoreceptor unit of *Rhodopseudomonas viridis. EMBO J.* 3:777–783.

Sundström, V., V. Pullertis, and R. van Grondelle. 1999. Photosynthetic light-harvesting: reconciling dynamics and structure of purple bacterial LH2 reveals function of photosynthetic unit. *J. Phys. Chem. B.* 103: 2327–2346.

van Burgel, M., D. A. Wiersma, and K. Duppen. 1995. The dynamics of one-dimensional excitons in liquids. *J. Chem. Phys.* 102:20–33.

van Grondelle, R. 1985. Excitation energy transfer, trapping and annihilation in photosynthetic systems. *Biochim. Biophys. Acta.* 811:147–195.

van Grondelle, R., J. P. Dekker, T. Gillbro, and V. Sundström. 1994. Energy transfer and trapping in photosynthesis. *Biochim. Biophys. Acta.* 1187:1–65.

van Mourik, F., R. W. Visschers, and R. van Grondelle. 1992. Energy transfer and aggregate size effects in the inhomogeneously broadened core light-harvesting complex of *Rhodobacter sphaeroides. Chem. Phys. Lett.* 193:1–7.

Walz, T., S. J. Jamieson, C. M. Bowers, P. A. Bullough, and C. N. Hunter. 1998. Projection structures of three photosynthetic complexes from *Rhodobacter sphaeroides*—LH2 at 6 angstrom, LH1 and LH-RC at 25 angstrom. *J. Mol. Biol.* 282:833–845.

Wu, H.-M., M. Rätsep, I.-J. Lee, R. J. Cogdell, and G. J. Small. 1997a. Exciton level structure and energy disorder of the B850 ring of the LH2 antenna complex. *J. Phys. Chem. B.* 101:7654–7663.

Wu, H.-M., N. R. S. Reddy, and G. J. Small. 1997b. Direct observation and hole burning of the lowest exciton level (B870) of the LH2 antenna complex of *Rhodopseudomonas acidophila* (strain 10050). *J. Phys. Chem. B.* 101:651–656.

Xiao, W., S. Lin, A. K. W. Taguchi, and N. W. Woodbury. 1994. Femtosecond pump-probe analysis of energy and electron transfer in photosynthetic membranes of *Rhodobacter capsulatus. Biochemistry.* 33: 8313–8322.

Zhang, W. M., T. Meier, V. Chernyak, and S. Mukamel. 1998a. Exciton-migration and three-pulse femtosecond optical spectroscopies of photosynthetic antenna complexes. *J. Chem. Phys.* 108:7763–7774.

Zhang, W. M., T. Meier, V. Chernyak, and S. Mukamel. 1998b. Simulation of three-pulse echo and fluorescence depolarization in photosynthetic aggregates. *Philos. Trans. R. Soc. Lond. A.* 356:405–419.

Zuber, H., and R. A. Brunisholz. 1991. Structure and function of antenna polypeptides and chlorophyll-protein complexes: principles and variability. *In* Chlorophylls. H. Scheer, editor. CRC Press, Boca Raton, FL. 627–703.

Zuber, H., and R. J. Cogdell. 1995. Structure and organization of purple bacterial antenna complexes. *In* Anoxygenic Photosynthetic Bacteria. R. E. Blankenship, M. T. Madigan, and C. E. Bauer, editors. Kluwer Academic Publishers, Dordrecht, Boston, and London. 315–348.